Archives of Biochemistry and Biophysics 581 (2015) 19–24

Contents lists available at ScienceDirect

Archives of Biochemistry and Biophysics

journal homepage: www.elsevier.com/locate/yabbi

Review

Overview and future of single particle electron cryomicroscopy

Richard Henderson

MRC Laboratory of Molecular Biology, Francis Crick Avenue, Cambridge CB2 0QH, UK

ARTICLE INFO

Article history:
Received 10 February 2015
Available online 18 March 2015

Keywords:
Electron cryomicroscopy
CryoEM
Single particle
Amorphous ice
Radiation damage
Beam-induced movement

ABSTRACT

Electron cryomicroscopy (cryoEM) has experienced a quantum leap in its capability in recent years, due to improved microscopes, better detectors and better software. It is now possible to obtain near-atomic resolution 3D density maps of macromolecular assemblies using single particle cryoEM without the need for crystals. Although this recent progress has produced some outstanding achievements, we have still only partly realised the full potential of single particle cryoEM. If one or two remaining problems can be solved, it will become an even more powerful method in structural biology that should closely approach the limit of what is theoretically possible.

Origins

Probably the most important step in the development of electron cryomicroscopy came from the work of Jacques Dubochet's group at EMBL during the period 1980–1982. They studied the behaviour of thin films of water when cooled to different temperatures and at different rates. They worked out how to freeze rapidly very thin films of biological macromolecules, so that they ended up embedded in amorphous ice at liquid nitrogen temperature [1]. An excellent review [12] described their approach in detail and included beautiful images of the many different specimens that they studied, including viruses, ribosomes and other structures with either point group or helical symmetry. It was clear then that the method had great promise and, as the many technical aspects have been improved, it has become more and more productive.

A micrograph (Fig. 1) that appeared on the front cover of Nature in 1984 showed a field of view with many intact (plus a few broken) adenovirus particles. Adenovirus biology was the life's work of Lennart Philipson who had become the second Director at EMBL in 1982, just as the work of Dubochet's group had emerged, and this gave Dubochet strong support in Heidelberg. These adenovirus images could be analysed to derive the 3D structure of icosahedral viruses using methods developed in the 1970s [9], resulting in a structure that reached a resolution of about 35 Å [36]. Technical improvements over the next 25 years allowed Hong Zhou and his colleagues at UCLA to obtain a 3D structure of adenovirus with a resolution of 3.6 Å [21], using a 300 keV microscope with images recorded on film. Fig. 2 shows part of one of their images of adenovirus and some regions of density from their map. So, what enabled the resolution to improve by a factor of ~10, corresponding to over a thousand times more information in 3D?

A principal reason is that the electron microscopes have been greatly improved during this time, partly from the work of individuals but mostly because the manufacturers, such as FEI (formerly Philips), JEOL and Hitachi, have responded to the demands of researchers for better equipment. The accelerating voltage has increased from 120 kV as it was in 1982 to 300 kV, or sometimes even 400 kV. The thermionic emission electron guns with a tungsten filament have been superseded by electron guns with field emission tips, giving 500-fold increases in brightness and consequently in spatial coherence. The temperature of the electron source cathodes has also dropped from ~3000 °C to ~1800 °C with an accompanying reduction in the electron energy spread and consequent increase in temporal coherence. At the same time, the microscope vacuum around the cold specimens has been improved so that the build-up of ice contamination has been greatly reduced, allowing specimens to remain in the microscope for days rather than hours. This allows thousands of images to be recorded from the same specimen in a single session, rather than just a few dozen. Finally, the stability of the cold stages has also been greatly improved so that drift rates, due to temperature fluctuations, have been reduced from a few Ångstroms per second to less than 0.1 Å/s. Automation has also played its part, with long sessions on the microscope requiring overnight working being replaced by computer-controlled data acquisition using programs such as Leginon [34] or FEI's EPU system.

E-mail address: rh15@mrc-lmb.cam.ac.uk

http://dx.doi.org/10.1016/j.abb.2015.02.036
0003-9861/

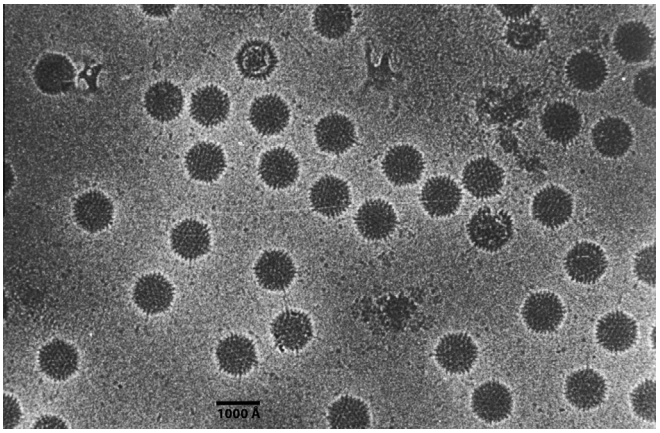

Fig. 1. Part of a cryoEM micrograph of adenovirus particles from the original paper on electron cryomicroscopy of viruses by Dubochet and his colleagues at EMBL [1]. Similar images, using 1980s technology produced a 3D model (not shown) of adenovirus at 35 Å resolution [36].

While a number of icosahedral virus structures were determined during the last 10 years at resolutions between 3 and 4 Å using images recorded on film, the 3D maps that were produced required the averaging of tens of thousands of single particle images, which corresponds to millions of asymmetric units. This amount of averaging was reminiscent of that required in electron crystallography of 2D crystals, which had also required the averaging of millions of asymmetric units to obtain 3D maps with 3–4 Å resolution. At the same time, one or two 3D structures of helical assemblies with resolutions in the 4–5 Å region were published, such as the bacterial flagellum [43] and the acetylcholine receptor [39]. Virtually all these higher resolution structures of icosahedral viruses, 2D crystal or helical arrays were obtained from electron micrographs recorded on film.

Recent developments

The two most significant recent developments, during the last 2–3 years (since 2012) have been the introduction of direct electron detectors, based on CMOS[1] (complementary metal oxide semiconductor) fabrication methods, and maximum likelihood algorithms in the computer programs for image processing.

The new detectors have a detective quantum efficiency (DQE) that is much higher at 300 keV than film, which was previously the best [24]. This increased DQE results in images with improved signal-to-noise ratio, which is always limited by the maximum electron dose permitted by radiation damage to the specimen. The consequences of radiation damage can be minimised by maintaining the specimen at low temperatures [38], cooled for example to liquid nitrogen or liquid helium temperature, but radiation damage cannot be avoided for organic or biological molecules. The detectors also read out the signal from the incident electrons in "rolling-shutter" mode, so no beam-blanking is required between frames. Thus, every exposure initially consists of a series of "movie" frames, which can simply be added together provided the specimen is not moving. However, by storing and processing the individual frames, it is possible to remove any residual stage drift due to temperature instabilities. It is also possible to compensate for beam-induced image blurring due to specimen charging and beam-induced physical motion of the specimen. With large enough structures, this processing of individual frames could be done for each particle, but for smaller structures the compensation of beam-induced motion can only be done for sub-regions of each image containing several particles.

There has been steady improvement in the performance of the computer programs for image processing as more and faster processing has allowed the development of more sophisticated algorithms. Maximum likelihood algorithms, in which accurate estimations of the signal and the noise levels in the data are used to refine the parameters, require significantly greater computational resources, so have not been implemented until recently. The X-ray crystallography community has used maximum likelihood methods for many years in programs such as SHARP, BUSTER and PHASER. Early applications to electron microscope projection images (i.e. not in 3D) were also developed by Fred Sigworth at Yale [33] and tested on projection images of 2D crystals [44]. Sjors Scheres has introduced maximum likelihood algorithms at the heart of RELION, a new package for single particle electron microscopy, with the name being derived from "REgularised LIkelihood OptimisatioN" [31]. His new program has produced significantly better structures than obtained previously using the same input data (e.g. [11]). At the same time Niko Grigorieff has made improvements to his Frealign package [23] and Steven Ludtke has made improvements to his EMAN2 package [37,8].

Together, these improved microscopes, better detectors and better software have produced a minor revolution in the resolution attainable in modern single particle cryoEM, described as a "resolution revolution" by Kuhlbrandt in a recent article [18].

This section concludes by showing three examples of recent 3D structures obtained using the new detectors, state-of-the-art microscopes and the new software. These are the mitochondrial ribosome [3], the TRPV1 capsaicin-receptor membrane channel [7,20] and the F420 hydrogenase [2], shown in Figs. 3–5 respectively.

Theoretical background

My own interests have been to try to analyse whether the images being acquired agree with what would be expected from theory. This was relatively easy for 2D crystals where the amplitudes in electron diffraction patterns could be compared with the strength of the Fourier components in images of the same 2D crystalline specimen. Using this approach, it was shown [16] that images of beam-sensitive 2D crystals, supported on a thin carbon film, such as monolayer paraffin ($C_{44}H_{90}$) or purple membrane had only about 4% of the expected contrast in the resolution range 4.0–4.5 Å, compared with 20% for the non-beam-sensitive vermiculite control. A subsequent review [14] showed that for ice-embedded helical assemblies such as tobacco mosaic virus (TMV), the effective loss of contrast in cryoEM images was even worse. The cause of the contrast loss was ascribed to a combination of build-up of positive charge on the specimen during the exposure due to secondary electron emission, and physical movement caused by radiation damage and subsequent bond breakage and release of radiation fragments such as hydrogen, oxygen and methane, which are gases at liquid nitrogen temperature. This led to a review [15] in which an attempt was made to calculate from first principles, with some simplifying assumptions, the size of the smallest particle that would allow its orientation to be determined from single particle cryoEM images, if perfect images could be obtained that were limited only by radiation damage and not charging or movement. In addition, the review suggested that about 12,000 single particles, less if they had internal symmetry, would be required to obtain enough information to calculate the 3 Å resolution structure. The number of particles required was also independent of the particle size or molecular weight. For large particles, each single particle image has more contrast than for small particles so fewer images are required to determine the projection structure to a desired

[1] *Abbreviations used:* cryoEM, electron cryomicroscopy; CMOS, complementary metal oxide semiconductor; DQE, detective quantum efficiency; TMV, tobacco mosaic virus; RELION, REgularised LIkelihood OptimisatioN.

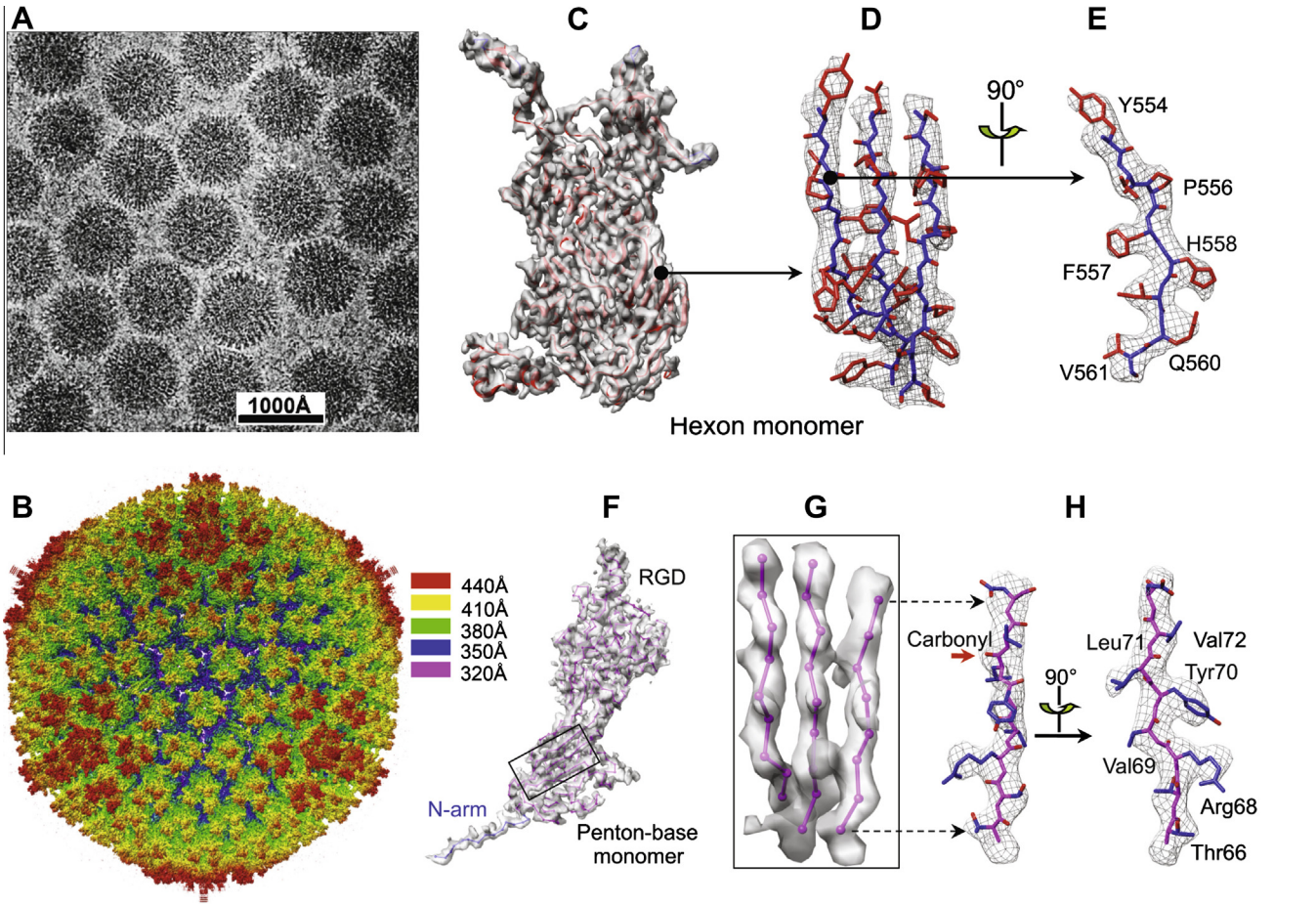

Fig. 2. Collage showing part of a micrograph, the overall structure and some selected density regions from the 3.6 Å map of the structure of adenovirus, using the technology of film in 2010, before the availability of the new CMOS detectors [21,22]. The individual panels are taken from Figs. 1A, S1A and S2 of Liu et al. [21] and from Fig. 1(c) and (d) from Liu et al. [22]. (A) CryoEM image of adenovirus virions recorded on Kodak SO163 film in an FEI Titan Krios electron cryo-microscope operated at 300 kV at liquid-nitrogen temperature. (B) 3D reconstruction of the adenovirus at 3.6 Å resolution. (C–E) A hexon monomer (C) extracted from (B) and with its atomic model (ribbons) superimposed on the density map (semi-transparent grey). (D) Representative enlargements of a β sheet showing separation of strands. (E) One of its three strands is rotated to show side chains (labelled) that are perpendicular to the β sheet. In (D) and (E), densities are shown as mesh, and atomic models are displayed using sticks. (F–H) A penton-base monomer extracted from (B). (F) Superposition of the cryoEM density map (semi-transparent) and the backbone of the atomic model (magenta sticks) of penton-base protein, including the 'N-arm' region (blue sticks). (G) Representative enlargement of a β sheet [boxed region in (F)] showing separation of strands. (H) Stick model of one strand superimposed on its density map (mesh) showing a representative carbonyl (red arrow) density and 90° rotated to show side chains (labelled) that are perpendicular to the β sheet.

accuracy. On the other hand, large particles require more views to sample reciprocal space adequately, according to the $\pi D/d$ formula of Crowther et al. [10], and these two effects cancel out precisely. The estimate of 12,000 particles was later revised to ~1400 [13] and then to 600 [27] when it was realised that the earlier signal-to-noise 3σ criterion was more stringent than had been shown to be adequate in protein crystallography.

Comparison between theory and practice

Once the new movie cameras were available, it became possible to study beam-induced specimen motion in more detail. It was found that the ice-embedded macromolecules on electron irradiation moved not only parallel to the plane of the thin ice film (i.e. in the x and y directions relative to the z-direction of the electron beam) but also vertically due to doming [42] or more complex motions. This changed the particle orientations during the exposure sometimes by several degrees [17,5,6]. The motion was found to be greater during the early part of the low-dose exposure, decreasing as the specimen stabilised. Most recently this has led to a number of improved protocols for image processing that effectively deblur the movie frames [19,40,41,4,28,32]. Fig. 6 shows the signal in different movie frames for 4 different structures. It is clear that the information that is presently used to determine a single particle cryoEM structure does not come from the first few electrons/Å**2, but from the frames recorded between 3–4 and 10–15 electrons/Å**2.

Many studies of electron diffraction from 2D crystals, such as bacteriorhodopsin, have shown that the diffraction spots fade faster at high resolution than at low resolution. For example, Stark et al. [35] showed that the 7 Å resolution spots, for specimens at liquid nitrogen temperature, faded to roughly half their intensity at 3 electrons/Å**2, but the 3 Å resolution spots had faded to 1% of their initial intensity at the same 3 electrons/Å**2 dose. This difference is extremely interesting. Effectively 99% of the diffraction power from beam-sensitive organic or biological specimens is lost after an exposure to 3 electrons/Å**2, yet in single particle cryoEM images, these movie frames can be discarded with no effect or even a beneficial effect on the resolution of the subsequent map. Clearly this apparent paradox is sending the important message that the beam-induced specimen motion, triggered by electron irradiation, is still a fundamental problem and a barrier to progress. Until a cure to eliminate or minimise it is found, electron cryomicroscopy will not realise its full potential.

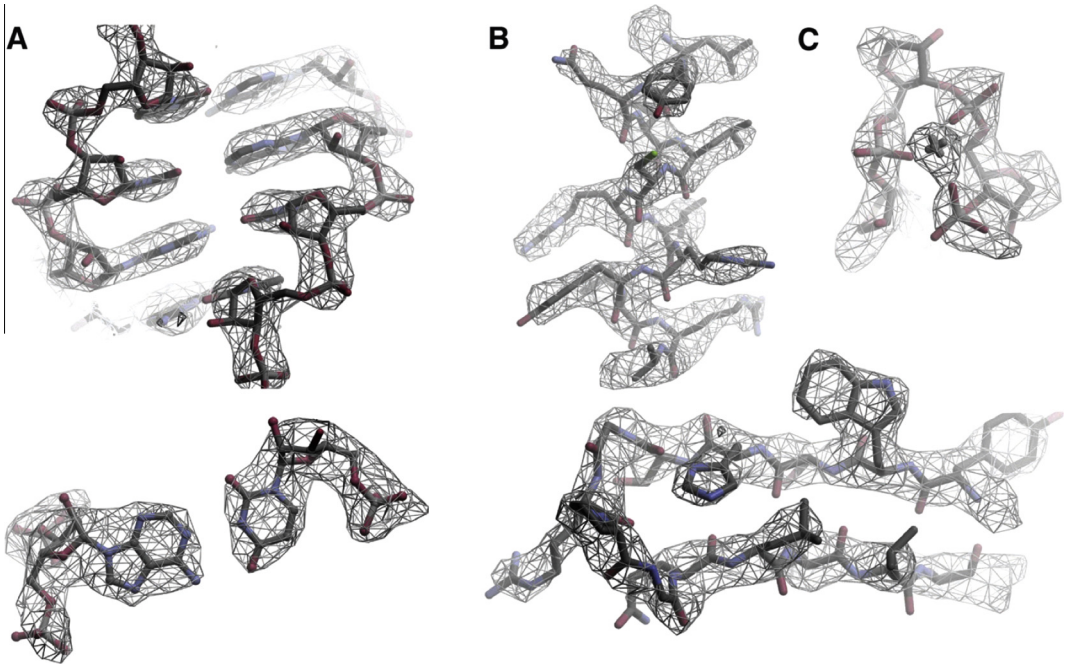

Fig. 3. Three selected regions of a cryoEM density map of the mitochondrial ribosome at ~3 Å resolution, showing a region of double-stranded RNA with Watson–Crick base pairs (A), as well as regions of α-helix (B) and β-hairpins with well-resolved backbone and side chains. A magnesium ion (C) is seen at top right. This figure is reproduced from Fig. 1 in Amunts et al. [3].

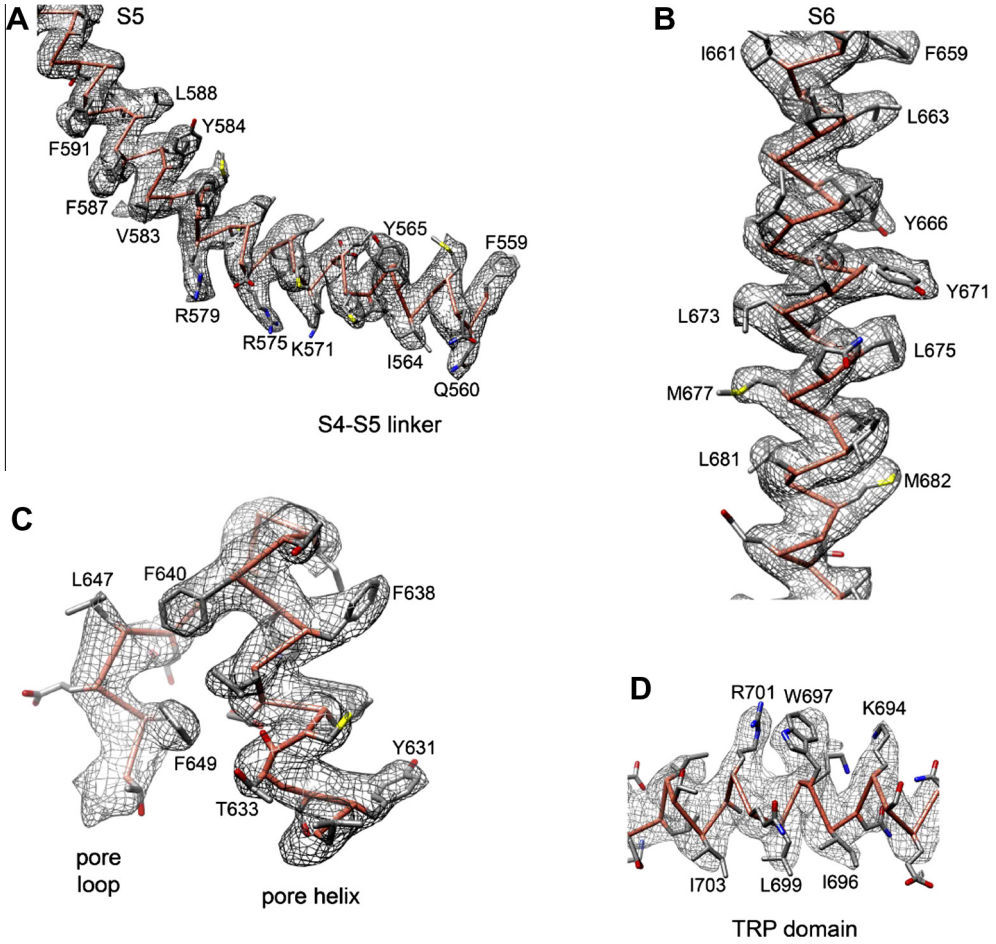

Fig. 4. α-Helical regions of the structure of the capsaicin TRPV1 channel [7,20], at a resolution of around 3.5 Å. This figure is reproduced from Extended Data Fig. 9a–d in Liao et al. [20].

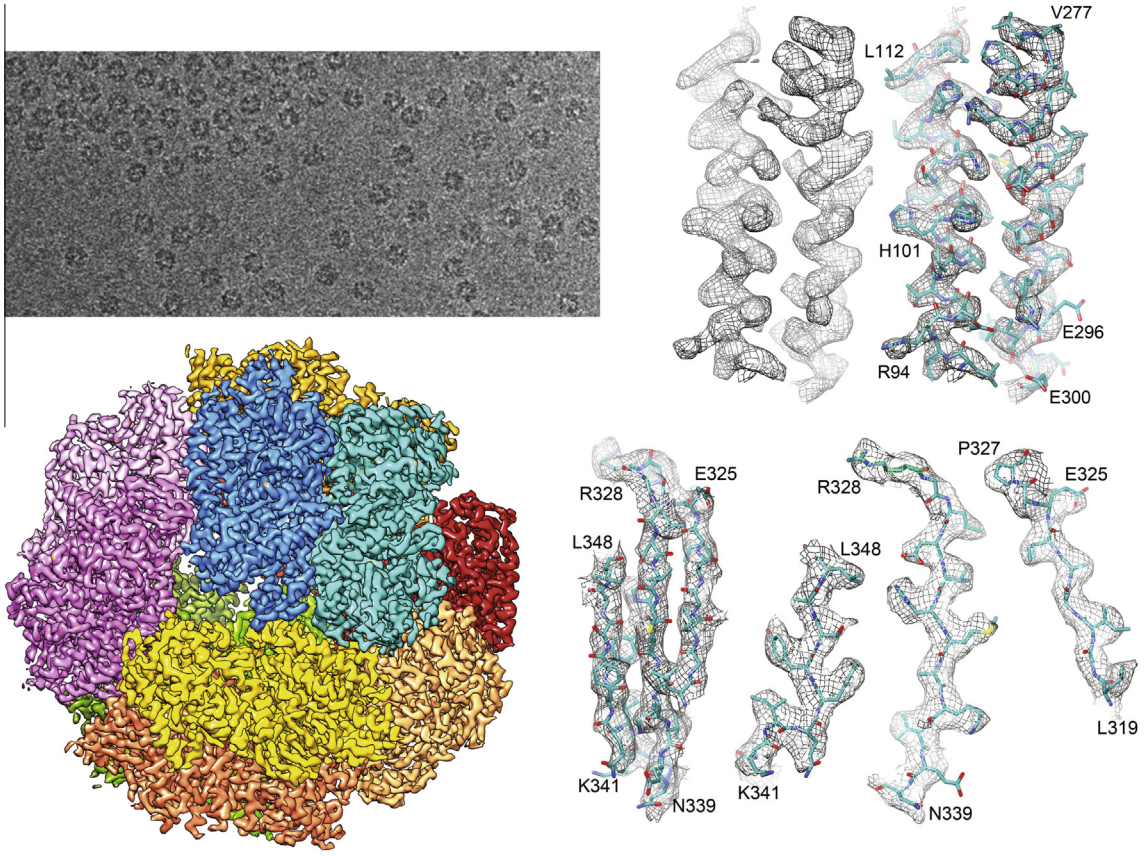

Fig. 5. Part of a micrograph, the overall structure and some density regions showing α-helices, β-sheets and side chains in the hydrogenase enzyme F420 [2]. The panels in this collage have been reproduced from Fig. 1A (selected region), 4, 7 and 8 in Allegretti et al. [2].

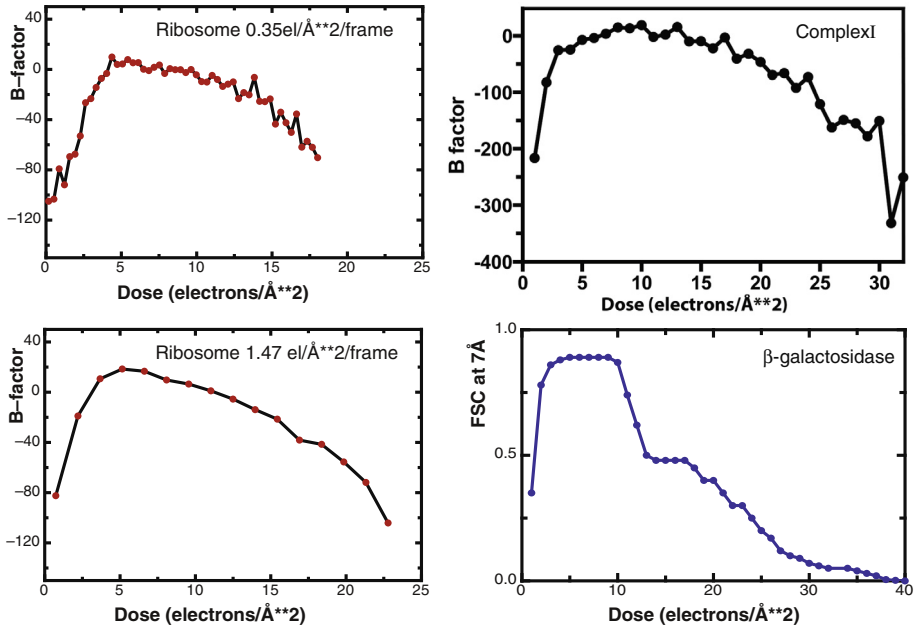

Fig. 6. Information content in different movie frames, displayed using a plot of relative B-factors [32] or information content around 7 Å resolution from a Fourier Shell Correlation plot [40]. The two panels on the left of this figure were kindly provided by Dr. Scheres using the procedure described in Scheres [32]. The panel at top right was kindly provided by Dr. Vinothkumar [41]. The panel at bottom right is reproduced from Vinothkumar et al. [40,41] Fig. 3B.

Causes of beam-induced specimen motion

The origins of the observed beam-induced motion need to be understood before they can be cured. At this point in early 2015, two distinct types of beam-induced motion are known to occur. The first consists of the motion of ~2000 Å wide regions [17,5,6] that move as an entity with all the macromolecules within the area moving as a relatively intact unit. We assume this is due to the release of stresses in the thin frozen film that are trapped immediately upon the initial plunge-freezing of the specimen, due to the expansion of water to form amorphous ice and the differential contraction of the ice, metal grid bars and supporting carbon film as the whole specimen is cooled from room temperature to the temperature of liquid nitrogen. The stresses can be annealed away as soon as the frozen film is irradiated, since irradiation allows the ice film to flow in a similar way to a fluid. The second type of beam-induced motion can be described as pseudo-Brownian motion in which the particles move randomly as they are pushed around by the random motion of the irradiated water molecules, which in turn move by a few Ångstroms at doses of a few electrons/Ångstrom**2 [25].

The first type of beam-induced motion can, in principle and to a great extent in practice, be corrected by subsequent computer-based image processing to align the individual frames of the movies collected using the new CMOS detectors [19,40,41,4,28,32]. The second type of pseudo-Brownian motion cannot be avoided but fortunately seems to be small enough [25] to be of minor significance for the practice of single particle cryoEM structure determination. Finally, it is possible that there are other types of deleterious beam-induced specimen motion that we have not yet identified, or other technical problems that cause blurring of cryoEM images due to specimen charging. New types of specimen support will help to overcome some of these problems [29,30,26].

Future prospects

In conclusion there are two principal remaining problems. First, we need to increase detector DQE to nearer 100% right out to the highest resolution on the detector (Nyquist) so that the images are recorded with no technical losses due to inadequate solutions to the remaining problems of detector physics. Second, we need to solve or at least ameliorate the problem of beam-induced movement. If both of these problems could be solved, then the future of electron cryomicroscopy will indeed be even brighter than it is at present. Single particle 3D structures will be able to be determined on smaller complexes, using fewer particles, to higher resolution or with more multiple states than at present. Beyond that, there is still further scope for improvement by reducing the specimen temperature from liquid nitrogen to liquid helium. At present, this is ruled out by the fact that the beam-induced motion at liquid helium temperatures produces images with much worse beam-induced blurring than at liquid nitrogen temperature, but if the specimen motion can be reduced, then liquid helium images might well produce a further small improvement, perhaps by another factor of two in radiation dose, as shown in comparative studies of the effects of radiation damage in fading of diffraction spots from 2D crystals [35].

Acknowledgments

I would like to thank Prof. Hong Zhou for providing Fig. 2, and Drs. Vinothkumar and Scheres for the plots used in Fig. 6. This article was prepared with support from the Medical Research Council, United Kingdom Grant No. U105184322.

References

[1] M. Adrian, J. Dubochet, J. Lepault, A.W. McDowell, Nature 308 (1984) 32–36.
[2] M. Allegretti, D.J. Mills, G. McMullan, W. Kuhlbrandt, J. Vonck, Elife 3 (2014) e01963.
[3] A. Amunts, A. Brown, X.C. Bai, J.L. Llácer, T. Hussain, P. Emsley, Fei. Long, G. Murshudov, S.H.W. Scheres, V. Ramakrishnan, Science 343 (2014) 1485–1489.
[4] X.C. Bai, I.S. Fernandez, G. McMullan, S.H. Scheres, Elife 2 (2013) e00461.
[5] A.F. Brilot, J.Z. Chen, A. Cheng, J. Pan, S.C. Harrison, C.S. Potter, B. Carragher, R. Henderson, N. Grigorieff, J. Struct. Biol. 177 (2012) 630–637.
[6] M.G. Campbell, A. Cheng, A.F. Brilot, A. Moeller, D. Lyumkis, D. Veesler, J. Pan, S.C. Harrison, C.S. Potter, B. Carragher, Grigorieff, Structure 20 (2012) 1823–1828.
[7] E. Cao, M. Liao, Y. Cheng, D. Julius, Nature 504 (2013) 113–118.
[8] Y. Cong, S.J. Ludtke, Single particle analysis at high resolution, Methods in Enzymology, vol. 482B, 2010, pp. 211–235.
[9] R.A. Crowther, Philos. Trans. R. Soc. London 261 (1971) 221–230.
[10] R.A. Crowther, D.J. DeRosier, A. Klug, Proc. R. Soc. A 317 (1970) 3190340.
[11] A. des Georges, Y. Hashem, A. Unbehaun, R.A. Grassucci, D. Taylor, C.U.T. Hellen, T.V. Pestova, J. Frank, Nucleic Acids Res. 42 (2014) 3409–3418.
[12] J. Dubochet, M. Adrian, J.-J. Chang, J.-Cl. Homo, J. Lepault, A.W. McDowell, P. Shultz, Q. Rev. Biophys. 21 (1988) 129–228.
[13] R.M. Glaeser, J. Struct. Biol. 128 (1999) 3–14.
[14] R. Henderson, Ultramicroscopy 46 (1992) 1–18.
[15] R. Henderson, Q. Rev. Biophys. 28 (1995) 171–193.
[16] R. Henderson, R.M. Glaeser, Ultramicroscopy 16 (1985) 139–150.
[17] R. Henderson, S. Chen, J.Z. Chen, N. Grigorieff, L.A. Passmore, L. Ciccarelli, J.L. Rubinstein, R.A. Crowther, P.L. Stewart, P.B. Rosenthal, Mol. Biol. 413 (2011) 1028–1046.
[18] W. Kuhlbrandt, Science 343 (2014) 1443–1444.
[19] X. Li, P. Mooney, S. Zheng, C.R. Booth, M.B. Braunfeld, S. Gubbens, D. Agard, Y. Cheng, Nat. Methods 10 (2013) 584–590.
[20] M. Liao, E. Cao, D. Julius, Y. Cheng, Nature 504 (2013) 107–112.
[21] H. Liu, L. Jin, S.B.S. Koh, I. Atanasov, S. Schein, L. Wu, Z.H. Zhou, Science 329 (2010) 1038–1043.
[22] H. Liu, L. Wu, Z.H. Zhou, Mol. Biol. 406 (2011) 764–774.
[23] D. Lyumkis, A.F. Brilot, D.L. Theobald, N. Grigorieff, J. Struct. Biol. 183 (2013) 377–388.
[24] G. McMullan, A.R. Faruqi, D. Clare, R. Henderson, Ultramicroscopy 147 (2014) 156–163.
[25] G. McMullan, K.R. Vinothkumar, R. Henderson, Thon rings from amorphous ice and implications of beam-induced Brownian motion in single particle electron cryo-microscopy, Ultramicrosopy (2015) (in press).
[26] J.R. Meyerson, P. Rao, J. Kumar, S. Chittori, S. Banerjee, J. Pierson, M.L. Mayer, S. Subramaniam, Sci. Rep. 4 (2014) 7084, http://dx.doi.org/10.1038/srep07084.
[27] P.B. Rosenthal, R. Henderson, J. Mol. Biol. 333 (2003) 721–742.
[28] J.R. Rubinstein, M.A. Brubake, Alignment of cryo-EM movies of individual particles by gradient-based optimization (2014). arXiv:1409.6789.
[29] C.J. Russo, L.A. Passmore, Nat. Methods 11 (2014) 649–652.
[30] C.J. Russo, L.A. Passmore, Science 346 (2014) 1377–1380.
[31] S.H.W. Scheres, J. Struct. Biol. 180 (2012) 519–530.
[32] S.H.W. Scheres, Elife 3 (2014) e03665.
[33] F.J. Sigworth, J. Struct. Biol. 122 (1998) 328–339.
[34] S.M. Stagg, G.C. Lander, J. Pulokas, D. Fellmann, A. Cheng, J.D. Quispe, S.P. Mallick, R.M. Avila, B. Carragher, C.S. Potter, J. Struct. Biol. 155 (2006) 470–481.
[35] H. Stark, F. Zemlin, C. Boettcher, Ultramicroscopy 63 (1996) 75–79.
[36] P.L. Stewart, R.M. Burnett, M. Cyrklaff, S.D. Fuller, Cell 67 (1991) 145–154.
[37] G. Tang, L. Peng, P.R. Baldwin, D.S. Mann, W. Jiang, I. Rees, S.J. Ludtke, J. Struct. Biol. 157 (2007) 38–46.
[38] K.A. Taylor, R.M. Glaeser, Science 186 (1974) 1036–1037.
[39] N. Unwin, J. Mol. Biol. 346 (2005) 967–989.
[40] K.R. Vinothkumar, G. McMullan, R. Henderson, Structure 22 (2014) 621–627.
[41] K.R. Vinothkumar, J. Zhu, J. Hirst, Nature 515 (2014) 80–84.
[42] E.R. Wright, C.V. Iancu, W.F. Tivol, G.J. Jensen, J. Struct. Biol. 153 (2006) 241–252.
[43] K. Yonekura, S. Maki-Yonekura, K. Namba, Nature 424 (2003) 643–650.
[44] X. Zeng, H. Stahlberg, N. Grigorieff, J. Struct. Biol. 160 (2007) 362–374.